THERMAL-HYDROLOGICAL-MECHANICAL MODEL FOR FRACTURE PROPAGATION, FLUID FLOW, AND TRANSPORT IN POROUS ROCK

Daisuke Asahina, Jim Houseworth, and Jens Birkholzer

Earth Sciences Division
Lawrence Berkeley National Laboratory
Berkeley, CA 94720, USA
e-mail: dasahina@lbl.gov

ABSTRACT

Understanding thermal-hydrologic-mechanical (THM) behavior in geomaterials (e.g., porous rock), including fracture propagation, is key for many engineering underground applications such as high-level radioactive waste disposal, geothermal energy recovery (e.g., enhanced geothermal systems), petroleum recovery (e.g., shale gas and oil extraction), and geologic CO_2 sequestration (cap-rock fracturing and leakage). In this paper, a numerical modeling method for coupled THM processes, including fracture formation and evolution is presented. The method is facilitated by a three-dimensional (3D) Voronoi-based discretization technique, capable of representing discrete fractures and fracture damage development within a permeable rock matrix. This approach is illustrated with examples of hydromechanical coupled processes and fracture formation. Additional computational examples are also given for flow and transport processes in a fractured, permeable rock.

INTRODUCTION

Geomechanical processes are known to play an important role in hydrogeological behavior (Neuzil, 2003). Linkage between mechanics and hydrogeology occurs in two fundamental ways: through feedback between (1) rock strain, the geometry of pores and fractures, and their permeability and porosity; and (2) fluid pressure and rock mechanical stress. Although there have been great strides in the capability to compute problems involving hydromechanical coupling (e.g. Rutqvist et al., 2002), the problem of fracture initiation and propagation, and its impact on fluid flow processes, remains a major difficulty. Such problems are of particular importance for mechanically weak rock types such as clays and shales, because fractures can be relatively transient as a result of fracture self-sealing processes (Bastiaens et al., 2007). Such issues are important, e.g., for geo-environmental issues related to nuclear waste disposal (Bossart et al., 2004) and geologic carbon sequestration (Chiaramonte et al., 2008).

The first part of this paper covers a computational method applicable to 3D discrete fracture networks (DFNs). Fractures are considered as discrete features that interact with a porous rock matrix. Fracture configurations are mapped onto an unstructured, 3D Voronoi grid, which is based on a deterministic or random set of spatial points. DFNs are represented by the connections of the edge of a Voronoi cell. This methodology has the advantage that fractures can be more easily introduced in response to coupled hydromechanical processes, and it generally eliminates several potential issues associated with the geometry of DFN and numerical gridding. In this paper, the multiphase fluid-flow simulator, TOUGH2, is used to simulate flow and transport through discrete fractures in porous rock. Fracture cells are introduced at the boundaries of Voronoi cells so that flow and transport through a DFN interacting with a permeable rock matrix can be studied. Analytical solutions of saturated flow and transport through a single fracture are also **developed to verify the numerical results.**

The second part of this paper describes a newly developed coupling between a mechanical-damage model and TOUGH2, which allows us to compute fracture evolution as well as flow and transport through the fractured porous rock, thus accounting for dynamically changing THM conditions. Elastic response and fracture development is modeled by the mechanical-damage model based on the rigid-body-spring

network (RBSN). Spring constants are related to elastic rock mechanical properties, and fracture initiation is determined using a classical brittle approach. Both models share the same geometrical information from a 3D Voronoi grid and associated nodes, where the scalar field quantities (e.g., temperature, pressure, and saturation) and the generalized displacements are obtained by TOUGH2 and RBSN, respectively. Fractures propagate along Voronoi cell boundaries as THM-induced stresses evolve and exceed the material strength. In particular, an example application is presented that addresses the modeling of moisture-driven fracture problems, such as shrinkage cracking.

GRID GENERATION

Voronoi discretization

Voronoi discretization is an effective approach to partition a computational domain into an unstructured grid. The defining characteristic of the Voronoi cell is that all locations within the cell lie closer to the associated nodal point than to any other nodal point. In this study, the procedure of Voronoi discretization starts with nodal point insertion. Nodal points are sequentially placed into the domain by a pseudo-random number generator. The use of a random point set simplifies mesh generation and increases flexibility in the model geometry. Two inputs, the dimensions of the computational domain and a minimum allowable distance l_m between nodes, are prescribed to control the mesh size. The domain is eventually saturated through a set of points with the l_m constraint. By connecting these nodal points, the Delaunay tessellation is generated, after which the dual Voronoi tessellation is constructed. More details about Voronoi discretization techniques can be found in Asahina and Bolander (2011).

Discrete fracture representation

In this study, fractures are considered as discrete features that interact with a porous rock matrix. An irregular Voronoi grid is used to represent the rock matrix as a basic material structure. Existing or newly generated fractures are directly mapped onto such a Voronoi grid. A discrete fracture is represented by a series of Voronoi cell boundaries (i.e., edges of polygon) as shown in Figure 1 for a two-dimensional (2D) case. Fracture geometric data (e.g., fracture orientation, length, width, and shape) can be obtained by field mapping or by computer-generated information based on statistical representation. A single fracture is represented as follows (Fig. 1):

- Discretize rock matrix based on an irregular Voronoi grid.
- Overlay a reference fracture on top of the Voronoi grid.
- Select node-node connections which cross the reference fracture. The Voronoi cell boundaries of such node connections are defined as a part of the discrete fracture.
- Connect all segments of the discrete fracture.

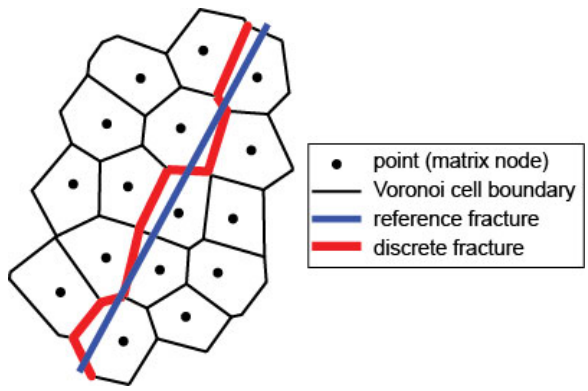

Figure 1. Mapping of a fracture geometry on top of an irregular Voronoi grid.

By repeating this process for a series of fractures, the modeler can generate a network of discrete fractures. The grid size must be carefully selected or scaled to obtain the required accuracy of discrete fracture representations. The advantages of this DFN generation method include: (1) simple activation and connection of new fractures, (2) automated treatment of fracture intersections, (3) capability to control mesh gradation (node density), and (4) straightforward extension to 3D geometry (Fig. 2). These advantages are especially beneficial when simulating fracture damage that develops into fracture networks. By automating the process of the proposed DFN approach, fracture intersections in 3D can be effectively generated. Figure 2a shows a fracture intersection mapped onto an irregular 3D Voronoi grid. The Voronoi cell boundaries tile the discrete fractures. This

facilitates the visualization of DFN, especially for 3D representation.

Alternatively, the Voronoi grid can be controlled by deterministic point selection to generate straight fractures with an intersection as shown in Figure 2b. Such grid generation, however, becomes cumbersome due to greater limitation on the point allocations around straight fractures, especially for fracture intersections in 3D.

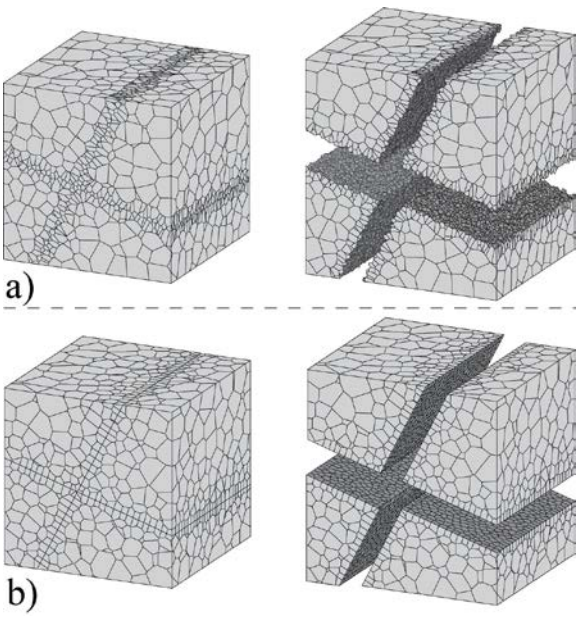

Figure 2. Fracture interface with the representation of DFN in 3D Voronoi grid: (a) irregular fractures, and (b) straight fractures.

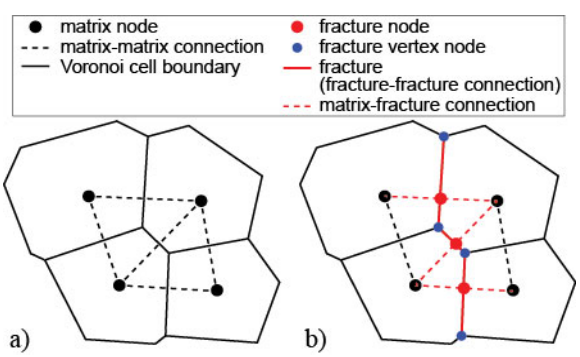

Figure 3. Node and connection in the TOUGH2 simulator: a) ordinary matrix nodes and connections, and b) new fracture nodes and connections.

Fracture nodes and connections in the TOUGH2 simulator

The simulations of flow and mass transport through discrete fractures, presented in a later section, are based on the TOUGH2 EOS7R simulator (Oldenburg and Pruess, 1995). As discussed in the preceding section, the DFN is explicitly represented at the Voronoi cell boundaries in a computational domain. To activate flow pathways along a discrete fracture, the fracture nodes and connections are newly introduced at the Voronoi cell boundary in addition to Voronoi cell nodes and connections for the rock matrix (Fig. 3). A new fracture node is inserted at the intersection of a Voronoi cell boundary and the original matrix-matrix connection. Then, the connection is generated between the fracture node and the adjacent matrix nodes. Also, the fracture vertex node is added to support fracture-fracture connections along the Voronoi cell boundary. These additional nodes and connections in the TOUGH2 simulator permit flow and transport through the DFN. Local fracture permeability and porosity are based on grid geometry and apertures, which can be either assigned as a pre-existing fracture or computed by a mechanical-damage model, as shown below. Performance of the proposed discrete fracture approach was tested against an analytical solution, as described in the following section.

NUMERICAL DISCRETE FRACTURE MODEL

A numerical discrete fracture model for a single fracture in a porous rock matrix is described here. Our current results focus on cases that can be verified with an analytical model, in which the fracture is a single linear feature that connects across the entire domain. The analytical model used here is an extension of the model developed by Houseworth (2006) for flow and transport in a single fracture. The model is capable of representing flow in the fracture, as well as flow in the matrix at an arbitrary oblique angle to the fracture. As for the original model (Houseworth, 2006), all transport mechanisms are represented except for longitudinal diffusion/dispersion.

The linear fracture model is a useful simplification because numerical results can be verified against the analytical model. These results, therefore, provide a reliable baseline for flow and transport behavior in more complex irregular fracture geometries. Two cases are presented below, involving flow parallel to the fracture and flow at an oblique angle to the fracture. The numerical solutions for flow and transport were conducted using TOUGH2 with the EOS7R module (Oldenburg and Pruess, 1995). Flow calculations were performed to establish steady-state flow fields that were used as an initial condition for the tracer-transport problem. For transport, an instantaneous point release of tracer was approximated by including at the beginning of the transport calculation tracer mass in one cell of the fracture. All problems were solved for a two-dimensional rectangular domain.

For parallel flow, the solution is symmetric with respect to the fracture orientation, so one boundary is taken along the fracture centerline. The domain is 10 m long and about 0.4 m in width, with a 0.015 m fracture half-aperture. Flow was computed using constant-pressure boundary conditions at each end of the 10 m long domain, and no-flow boundary conditions for the transverse direction. For the cross-flow case, the domain length is also 10 m, but symmetry is broken; therefore, the fracture is placed in the middle of the domain with a full aperture of 0.03 m and a domain width of about 1 m. For the cross-flow cases, a transverse pressure gradient of about 49,000 Pa/m is established. In all cases, the longitudinal pressure gradient is about 5000 Pa/m.

A uniform grid was used in the longitudinal direction (along the fracture axis). In the base case, a longitudinal grid spacing of 1 cm was used for the parallel flow condition and 2 cm for the cross-flow condition. Grid spacing laterally was 0.002 m near the fracture for these base cases, with coarser grids further from the fracture. There are three sensitivity cases each for parallel-flow and cross-flow conditions. For parallel flow, Sensitivity Case 1 uses a longitudinal grid spacing of 0.06 m, Case 2 a longitudinal grid spacing of 0.1 m, and Case 3 a longitudinal grid spacing of 0.1 m and a minimum lateral grid spacing of 0.01 m. For cross-flow, cases 1 and 3 use a longitudinal grid spacing of 0.1 m. Also, for the cross-flow base case and Case 3, fine gridding in the transverse direction was used for a larger region around the fracture than in the parallel-flow case. Hydrogeologic parameters are given in Table 1.

Table 1. Linear Fracture Simulation –Parameters.

Fracture permeability (m^2)	Matrix permeability (m^2)	Fracture aperture (m)	Fracture porosity	Matrix porosity	Diffusion coefficient (m^2/s)
2.4×10^{-15}	1.0×10^{-18}	0.03	0.087	0.2	1.0×10^{-11}

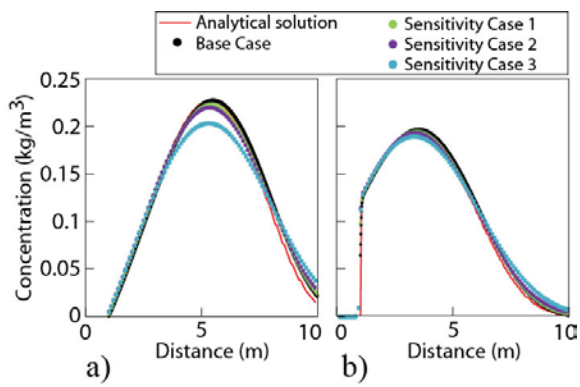

Figure 4. Mass concentration for parallel flow cases: (a) fracture concentration profile; and (b) matrix concentration profile about 2 cm from fracture.

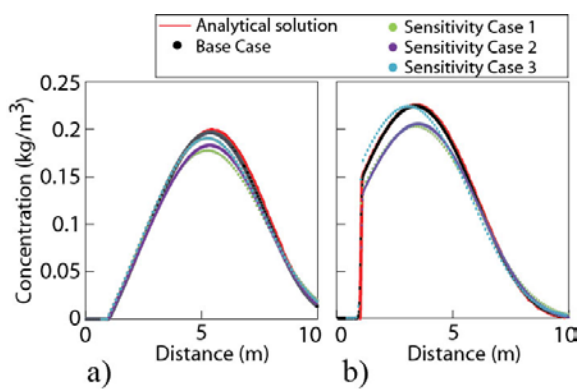

Figure 5. Mass concentration for cross-flow cases: (a) fracture concentration profile; and (b) matrix concentration profile about 2 cm from fracture.

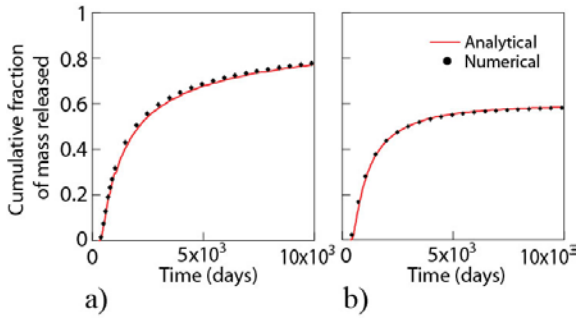

Figure 6. Cumulative mass arrival 4 m from release point: (a) parallel flow base case; and (b) cross-flow base case.

Results for the simulations are compared with analytical solutions in Figure 4 and 5. These figures show that the solution is most sensitive to grid refinement near the fracture and that longitudinal grids may be coarser. Additional transverse grid refinement in the matrix near the fracture appears to be necessary to achieve the same level of accuracy in the numerical model for the cases with cross flow. This appears to be a result of cross flow moving the peak mass concentration from the fracture and into the matrix. Steep concentration gradients are associated with the location of the peak mass concentration. The results also show that with sufficient grid refinement, numerical results can closely match the analytical solution, even though the numerical model includes longitudinal diffusion not represented in the analytical model. The numerical base-case results are compared with analytical results in Figure 6 for cumulative mass arrival at a downstream position 4 m from the release point. Cross flow is seen to slow longitudinal mass transport at later times. Cumulative mass arrival is a convenient metric for comparing results for linear and irregular fracture cases, which will be done in a future report.

MECHANICAL-DAMAGE MODEL

Elastic response and fracture development is modeled by the mechanical-damage model based on the rigid-body-spring concept of Kawai (1978). To provide a basic understanding of this modeling approach, an overview of the element formulation is given here. Geometry of the rigid-body-spring network (RBSN) is defined by the dual Delaunay tessellation of the nodal points. The basic unit of RBSN is a 1D lattice element consisting of a zero-size spring set located at the centroid of the Voronoi boundary (Fig. 7). Each node has six degrees of freedom for the 3D case. The spring set is formed from three axial springs and three rotational springs (referenced to local coordinate axes *n-s-t*) as shown in Figure 7 (the rotational springs have been omitted for clarity). The local spring coefficients are assigned according to

$$k_s = k_t = \alpha_1 k_n = \alpha_1 \alpha_2 E \frac{A_{ij}}{h_{ij}} \qquad (1)$$

in which E is the elastic modulus and A_{ij} is the area of the Voronoi boundary common to nodes i and j (Fig. 7). By adjusting α_1 and α_2 in accordance with experimental results, macroscopic modeling of both elastic constants (E and Poisson ratio, ν) is possible. The Voronoi scaling of the spring constants, A_{ij}/h_{ij}, , enables the method to be elastically homogeneous under uniform modes of straining. Such Voronoi scaling also serves energy conserving, grid-size-insensitive representations of tensile fracture. Details and indication of model accuracy can be found elsewhere (Bolander and Saito 1998, Asahina et al. 2011).

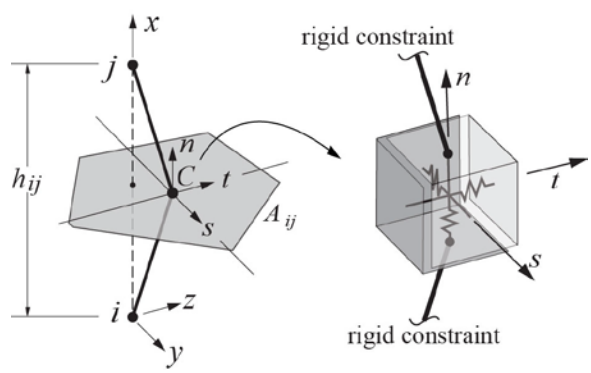

Figure 7. Typical lattice element with a zero-size spring set located at centroid C of facet area A_{ij}. Note that A_{ij} is tha Voronoi cell boundary and i and j is the neighboring Voronoi cell nodes (matrix nodes).

COUPLING OF TOUGH AND RBSN

Basic approach

TOUGH2 is coupled with RBSN to compute fracture damage development, as well as flow and transport through the fractured porous rock, accounting for dynamically changing THM conditions. The general procedure for the two-code coupling (hydraulic and mechanical code)

is similar to the earlier work of Rutqvist et al. (2002) who linked TOUGH2 to a commercial continuum-mechanics simulator, FLAC3D. In this paper, TOUGH2 is used to simulate the hydraulic quantities (e.g., temperature, pressure, and saturation), while RBSN accounts for the mechanical quantities (e.g., stress, strain, displacement, and damage). Such primary variables are coupled through simplified linear relationships or through nonlinear empirical expressions, which could be estimated by laboratory experiments with appropriate calibration. The main advantage of coupling TOUGH2 and RBSN is that both models share the same unstructured, 3D Voronoi grid and the same set of nodes. This greatly simplifies the process of exchanging primary variables between two codes. At the current stage, TOUGH2 and RBSN are linked through an external coupling module, which transfers the relevant variables at each time step. It is assumed that the local changes in hydraulic variables produce strain as follows:

$$\Delta\varepsilon_T = \alpha_T \Delta T \tag{2}$$

$$\Delta\varepsilon_s = \alpha_s \Delta S \tag{3}$$

$$\Delta\sigma = (\Delta\varepsilon_T + \Delta\varepsilon_s)E \tag{4}$$

where ε_T is the thermal strain, ε_s is the shrinkage/swelling strain, ΔT and ΔS is the change in temperature and saturation over the time step in one lattice element, respectively, α_T is the coefficient of thermal expansion, α_s is the moisture swelling coefficient, and σ is the stress. The hydraulic valuables, ΔT and ΔS, are taken as the average of two neighboring nodes *i* and *j*. At this stage of model development, hydro-mechanical coupling is based on one-way coupling, in which flow processes affect mechanical strain but mechanical behavior does not affect flow parameters (e.g., permeability, porosity). Since the flow parameters are constant during the simulations, mechanical stress is computed independent of fluid pressure. Examples in subsequence sections only explore the effect of saturation change on the mechanical response. Future work will include model development for more general approaches, such as two-way coupling and a fully coupled poro-elastic model.

Model validation

The TOUGH-RBSN simulator is validated by comparison with an independent simulation of the same process using TOUGH-FLAC (Rutqvist 2011). Consider a soil sample (20×20×20 mm) wetted at the bottom and fully confined mechanically, as shown in Figure 8. The model is discretized with 19 lattice elements and 20 nodes. Model boundaries are fully confined with mechanical fixed supports, and there is no flow across the boundaries except at the bottom water inlet. Both simulations were calibrated using data from an experiment that was part of the international collaborative model comparison project DECOVALEX III. The experiment was conducted for about 10 days at isothermal conditions (T=25°C). Initial saturation was 65% with elastic modulus of 60 MPa. From this information, the moisture swelling coefficient, α_s (Eq. 3), can be back-calculated to 0.238, as shown in Rutqvist et al. 2011.

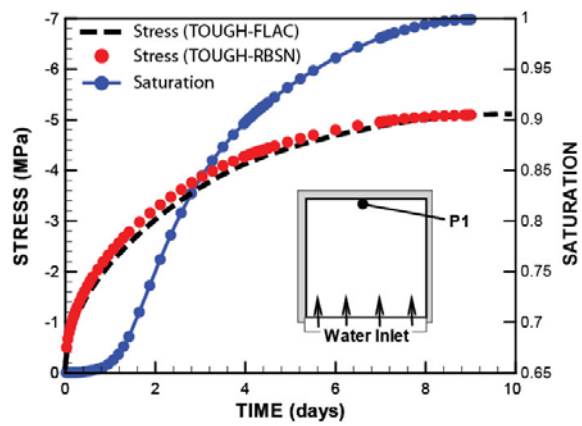

Figure 8. Time evolution of compressive stress and saturation at point P1 for simple swelling model.

Figure 8 shows the simulation results for time evolution of compressive stress and saturation. The hydraulic primary variables are accurately simulated by TOUGH2 as reported in Rutqvist et al. 2011. Stress increments are based on the saturation changes. The final stress is 5.12 MPa, which consists of 5 MPa (calibrated value) on top of the initial atmospheric stress of 0.12 MPa. Good agreement between the results simulated by TOUGH-RBSN and TOUGH-FLAC is achieved.

Simulation of desiccation cracking

Desiccation cracking is demonstrated by the TOUGH-RBSN simulator. Consider a slab subject to drying from the top surface. The initial saturation is set to 80%. The convective boundary condition is implemented by a thin layer of nodes at the top surface with prescribed nodal saturation (30%). Model boundaries are fixed at the bottom surface, whereas the vertical surfaces are only free to move in-plane. The vapor diffusion induced by saturation changes induces changes in strain within the mechanical element. In general, elements closest to the top surface shrink the most due to experiences the largest changes in saturation. The model is parameterized using hydrogeological and mechanical properties characteristic of expansive clay rock. Here, a classical brittle approach is used to break the lattice elements. Desiccation of expansive clay produces predominantly tensile stress fields due to the drying shrinkage. Tensile fracture is based on a measure of tensile stress calculated as $\sigma_R = F_R / A^P_{ij}$, where F_R is the resultant force acting on the element facet and A^P_{ij} is the projected area of the Voronoi cell boundary to the resultant force (Asahina et al. 2011). Simulation is conducted until no more major changes in the crack pattern are observed.

First, the insensitivity of the fracture pattern with respect to mesh size is studied using two different meshes with 2680 nodes and 297 nodes. Figure 9 shows the fracture pattern. The results show about the same number of major crack features, as well as similar spacing between the cracks.

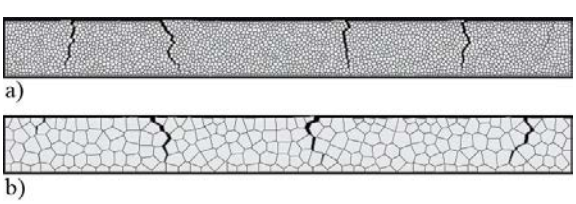

Figure 9. Fracture pattern with various mesh sizes: (a) fine mesh (2680 nodes), and (b) coarse mesh (297 nodes).

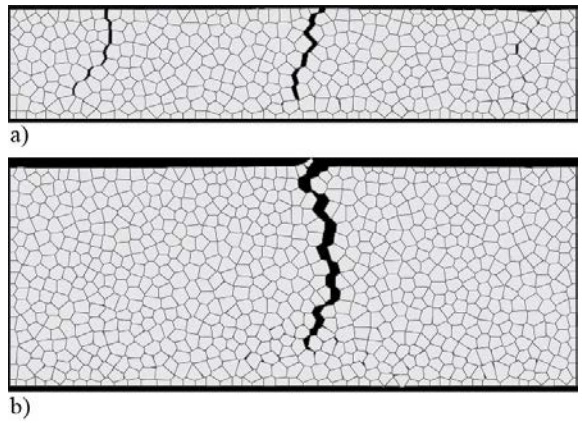

Figure 10. Fracture pattern with various thicknesses: (a) 20 mm, and (b) 40 mm.

Second, the basic aspect of fracture patterns is further studied for various slab thicknesses, as shown in Figure 10. Model thicknesses of 10 mm (Fig. 9b), 20 mm, and 40 mm are simulated. The resulting number of major cracks is about 4, 2, and 1, respectively. This general response, in which the distance between cracks increases with material thickness, has been observed in experiments (Colina and Roux, 2000). Bolander et al. (2007) have conducted a similar study for cement composite materials, where lattice-type models are used to calculate both mechanics and transport (e.g., moisture transport). Future work for desiccation cracking will involve more realistic simulations and quantitative comparisons with experimental data.

CONCLUSION

Computational methods are needed to address fracture initiation and propagation as a hydro-mechanical coupled process. The method reported here uses a finite volume method for flow processes and RBSN modeling for geomechanics. This allows for the coupling to be computed on a common grid using a random Voronoi gridding approach for two or three dimensions. The proposed methodology, in which fractures are placed along Voronoi cell boundaries, eliminates many issues regarding incorporating new fractures into a numerical grid, minimizing computational aspects associated with regridding. This allows for a more practical incorporation of fracture initiation and propagation into numerical models of coupled hydromechanical processes. Examples presented here have shown some of the applications of this computational strategy for modeling

hydrogeological and geomechanical coupled processes.

ACKNOWLEDGMENTS

The authors gratefully acknowledge Dr John E. Bolander at UC Davis for his suggestions and comments. We also thank Peter Persoff at LBNL for his careful review of a draft manuscript. Funding for this work was provided by the Used Fuel Disposition Campaign, Office of Nuclear Energy, of the U.S. Department of Energy under Contract Number DE-AC02-05CH11231 with Berkeley Lab.

REFERENCES

Asahina, D. and Bolander, J.E., Voronoi-based discretizations for fracture analysis of particulate materials, *Powder Technology*, *213*, 92–99, 2011.

Asahina, D., Landis, E.N., and Bolander, J.E., Modeling of phase interfaces during pre-critical crack growth in concrete, *Cement & Concrete Composites*, 33, 966-977, 2011.

Bastiaens W., Bernier, F., and Li, X.L., SELFRAC: Experiments and conclusions on fracturing, self-healing and self-sealing processes in clays, *Physics and Chemistry of the Earth* 32, 600–615, 2007.

Bolander, J.E. and Saito, S., Fracture analyses using spring networks with random geometry. *Eng Fract Mech*, 61, 569–91, 1998.

Bolander, J.E., Li, Z., and Yip, M., Restraint and cracking during non-uniform drying of cement composites, *Proceedings of the Transport Properties and Concrete Quality Workshop - Materials Science of Concrete*, American Ceramic Society, 123-140, 2007.

Bossart, P., Trick, T., Meier, P.M., and Mayor, J.-C., Structural and hydrogeological characterization of the excavation-disturbed zone in the Opalinus Clay (Mont Terri Project, Switzerland), *Applied Clay Science* 26 (2004) 429– 448.

Chiaramonte, L., Zoback, M.D., Friedmann, J., and Stamp, V., Seal integrity and feasibility of CO2 sequestration in the Teapot Dome EOR pilot: geomechanical site characterization, *Environ Geol* (2008) 54:1667–1675.

Colina, H. and Roux, S., Experimental model of cracking induced by drying shrinkage *Eur. Phys. J. E* 1, 189-194, 2000.

Houseworth, J.E., An analytical model for solute transport in unsaturated flow through a single fracture and porous rock matrix. *Water Resources Research*, 42, 2006

Kawai, T., New Discrete Models and their Application to Seismic Response Analysis of Structures, *Nuclear Engineering and Design* 48, 207-229, 1978.

Neuzil, C.E., Hydromechanical coupling in geologic processes, *Hydrogeology Journal* (2003) 11:41–83.

Oldenburg, C.M. and Pruess, K., EOS7R: Radionuclide Transport for TOUGH2, Lawrence Berkeley National Laboratory, LBL-34868, 1995.

Rutqvist, J., Wu, Y.-S., Tsang, C.-F., and Bodvarsson, G., A modeling approach for analysis of coupled multiphase fluid flow, heat transfer, and deformation in fractured porous rock, *International Journal of Rock Mechanics & Mining Sciences*, 39, 429–442, 2002.

Rutqvist, J., Ijiri, Y., and Yamamoto, H., Implementation of the Barcelona Basic Model into TOUGH–FLAC for simulations of the geomechanical behavior of unsaturated soils *Computers & Geosciences* 37, 751–762, 2011.